ADVANCING EARTH AND SPACE SCIENCES

JGR Atmospheres

RESEARCH ARTICLE
10.1029/2023JD039887

Key Points:

- Gravity wave temperature fluctuations, along with the Kelvin effect, rapidly reduce small ice crystal concentrations in anvil cirrus
- Waves and the Kelvin effect drive mass transfer from small to large crystals, consistent with the prevalence of bullet rosettes in anvils
- Wave effects on anvil cirrus microphysics are much more pronounced for low/warm anvils than for high/cold anvils

Correspondence to:
E. J. Jensen,
ericjj50@gmail.com

Citation:
Jensen, E. J., Kärcher, B., Woods, S., Krämer, M., & Ueyama, R. (2024). The impact of gravity waves on the evolution of tropical anvil cirrus microphysical properties. *Journal of Geophysical Research: Atmospheres*, *129*, e2023JD039887. https://doi.org/10.1029/2023JD039887

Received 24 AUG 2023
Accepted 8 DEC 2023

The Impact of Gravity Waves on the Evolution of Tropical Anvil Cirrus Microphysical Properties

E. J. Jensen[1,2], B. Kärcher[3], S. Woods[4], M. Krämer[5,6], and R. Ueyama[7]

[1]NOAA Chemical Sciences Laboratory, Boulder, CO, USA, [2]Cooperative Institute for Research in Environmental Sciences, University of Colorado, Boulder, CO, USA, [3]Deutsches Zentrum für Luft- und Raumfahrt (DLR Oberpfaffenhofen), Institut für Physik der Atmosphäre, Oberpfaffenhofen, Germany, [4]National Center for Atmospheric Research, Boulder, CO, USA, [5]Institute for Energy and Climate Research (IEK-7), Research Center Jülich, Jülich, Germany, [6]Institute for Atmospheric Physics (IPA), Johannes Gutenberg University, Mainz, Germany, [7]NASA Ames Research Center, Moffett Field, CA, USA

Abstract Anvil cirrus generated by deep convection covers large fractions of the tropics and has important impacts on the Earth's radiation budget and climate. In situ measurements made with high-altitude aircraft indicate a rapid transition in ice crystal size distributions and habits as anvil cirrus ages. We use numerical simulations to investigate the impact of high-frequency gravity waves on the evolution of anvil cirrus microphysical properties. The impacts of both monochromatic gravity waves and ubiquitous stochastic mesoscale temperature fluctuations are simulated. In both cases, the interplay between wave-driven temperature fluctuations, deposition growth/sublimation, and sedimentation causes accelerated removal of both small ice crystals (diameters less than about 10 μm) and large crystals (diameters larger than ≈30 μm). These changes are consistent with the observed evolution of anvil cirrus microphysical properties. The Kelvin effect (higher saturation vapor pressure over curved surfaces) is a critical factor in the anvil evolution, driving mass transfer from small to large ice crystals. The wave-driven decrease in ice concentration is much faster for typical anvil cirrus detrained at ≃11.5–12.5 km than for less frequent anvils at 15.5–17.5 km because of the strong temperature dependence of deposition growth and sublimation rates. The simulations also show that waves, along with the Kelvin effect, drive growth of mid-sized (5–20 μm) ice crystals, which is consistent with the observed transition to bullet rosette habits in aging anvil cirrus. We conclude that high-frequency gravity waves, which are generally not resolved in large-scale models, likely have important impacts on anvil cirrus microphysical properties and lifetimes.

1. Introduction

Tropical anvil cirrus produced by detrainment of ice crystals and humid air from the tops of deep convective cloud systems have a strong impact on the earth's radiation budget and climate. Anvil cirrus can persist for many hours or days (Luo & Rossow, 2004; Mace et al., 2006), and at any given time, anvil cirrus cover large fractions of the tropics (Yuan & Houze, 2010). A number of physical processes affect the evolution and lifetime of anvil cirrus, including sedimentation, synoptic-scale meteorology, mesoscale circulations driven by the convection and radiative heating within the anvils, radiatively-driven small-scale convection, turbulence, entrainment of dry air, and wind shear.

The lifetimes and radiative impacts of anvil cirrus depend on their microphysical properties, such as ice concentrations, size distributions, and habits. The limited available in situ measurements in active convection suggest broad ice crystal size distributions, with both abundant small ice crystals (diameters less than 20 μm), and large aggregates lofted by the convection (Gallagher et al., 2012; Jensen et al., 2009; Lawson et al., 2019). The abundant small ice crystals are expected since the strong convective updrafts drive supersaturation and homogeneous nucleation of ice crystals, and the production of numerous small crystals can continue all the way to the tops of the updrafts (Jensen & Ackerman, 2006). In contrast, the concentration of both small and large ice crystals in aged anvils is much lower than in the active convection and very fresh outflow (Gallagher et al., 2012; Jensen et al., 2009; Lawson et al., 2019; Woods et al., 2018). In addition to the evolution of ice crystal size distributions, the in situ measurements suggest a rapid transition in ice crystal habits from predominantly pristine crystals and aggregates in the tops of active convection to dominance by bullet rosettes in aged anvil cirrus (Gallagher et al., 2012; Lawson et al., 2019). The presence of bullet rosettes suggest that deposition growth has occurred in situ under supersaturated upper tropospheric conditions (Bailey & Hallett, 2004).

A number of modeling studies have shown that the ice crystals larger than ∼200 μm sediment out of the anvils within a few hours (Boehm et al., 1999; Gallagher et al., 2012; Jensen et al., 2018). However, it has not been clear what physical processes cause the apparent rapid loss of small ice crystals (and corresponding reduction in total ice concentration) in the early stages of anvil cirrus evolution. Differential sedimentation dilution will reduce ice concentrations, but sedimentation should have a negligible impact on the small ice crystals. Entrainment of dry air can also drive sublimation of small ice crystals.

A variety of observations, including high-altitude aircraft measurements, high-resolution radiosondes, and super-pressure balloon measurements have shown that temperature variability driven by gravity waves is essentially ubiquitous in the upper troposphere (Atlas & Bretherton, 2023; Karoly et al., 1996; Nath et al., 2009; Podglajen et al., 2016, 2017). A general background of stochastic mesoscale temperature fluctuations (MTFs) is present much of the time. In addition, deep convective systems themselves are an important source of upper tropospheric gravity waves in the tropics (Lane et al., 2001). Consistent with this fact, recent studies have shown that gravity wave activity is enhanced in the vicinity of deep convective systems (Atlas & Bretherton, 2023; Corcos et al., 2021; Podglajen et al., 2017).

A number of past studies have investigated the impact of gravity waves on cirrus clouds. These studies have generally focused on thin cirrus formed in situ in the tropical tropopause layer (TTL). Some of the previous investigations have focused on the relationship between gravity waves (particularly low frequency gravity waves such as Kelvin waves) and when/where TTL cirrus form (Atlas & Bretherton, 2023; Boehm & Verlinde, 2000; Immler et al., 2008; Kim et al., 2016). Another set of papers has focused on the impact of high-frequency waves on TTL cirrus via the dependence of ice concentrations produced by homogeneous freezing on cooling rate (Dinh et al., 2016; Jensen et al., 2010, 2016; Spichtinger & Krämer, 2013). Podglajen et al. (2018) used numerical simulations to show that monochromatic wave-driven temperature and vertical wind perturbations can lead to localization of ice crystals in a specific phase of the wave. Here, we investigate the impacts of wave-driven temperature fluctuations on the evolution of convectively-generated anvil cirrus in the tropical upper troposphere; that is, we focus on the processes occurring after ice nucleation has ceased. For this purpose, we use idealized one-dimensional simulations including deposition growth, sublimation, and sedimentation. We investigate the effects of both coherent, monochromatic waves and stochastic, MTFs. A key issue addressed in this study is the interplay between gravity waves and the Kelvin effect, which tends to destroy the small ice crystals.

Section 2 presents recent in situ measurements of active convection and aged anvil cirrus ice crystal size distributions. Section 3 describes the modeling approach. The evolution of anvil cirrus without wave effects is discussed in Section 4. The simulated impacts of monochromatic waves are presented in Section 5. In Section 6, we present Lagrangian calculations of individual ice crystal lifecycles in the anvil cirrus. In Section 7, we address the impact of ubiquitous MTFs on anvil cirrus microphysics. Lastly, Section 8 provides a summary and discussion of the results.

2. Deep Convection/Anvil Cirrus Ice Size Distribution Measurements

We start by presenting examples of deep convection and aged anvil cirrus ice crystal size distributions measured during recent high-altitude aircraft field campaigns. We present data from three campaigns: (a) the Airborne Tropical Tropopause Experiment (ATTREX), with NASA Global Hawk unmanned aircraft flights over the western Pacific during March 2014 (Jensen, Pfister, et al., 2017); (b) the Pacific Oxidants, Sulfur, Ice, Dehydration, and cONvection experiment (POSIDON) with NASA WB-57 flights over the western Pacific during October 2016; and (c) the Stratospheric and upper tropospheric processes for better climate predictions (StratoClim) campaign, with Geophysica flights over southern Asia during August 2016 (Krämer et al., 2020). During ATTREX and POSIDON, ice crystal size distributions were measured with two cloud probes: the Fast Cloud Droplet Probe (FCDP) (McFarquhar et al., 2007) measures the forward scattered laser light from individual ice crystals with sizes ranging from 1- to 50-μm diameter, and the 2D-S probe captures images of ice crystals with sizes ranging from 10 μm to 4 mm. For StratoClim, ice crystal size distributions were measured with the Novel Ice Experiment-Cloud Aerosol and Precipitation Spectrometer probe (Costa et al., 2017; Krämer et al., 2016), which is an aerosol and cloud probe mounted under the wing of Geophysica. It incorporates two instruments for measuring particle size distributions: particles with diameters ranging from 0.6 to 50 μm are measured with a Cloud and Aerosol Spectrometer using a technique similar to the FCDP. For measurements of particles 15–937 μm in diameter, a Cloud Imaging Probe greyscale is used, which utilizes the optical array probe technique. The ATTREX

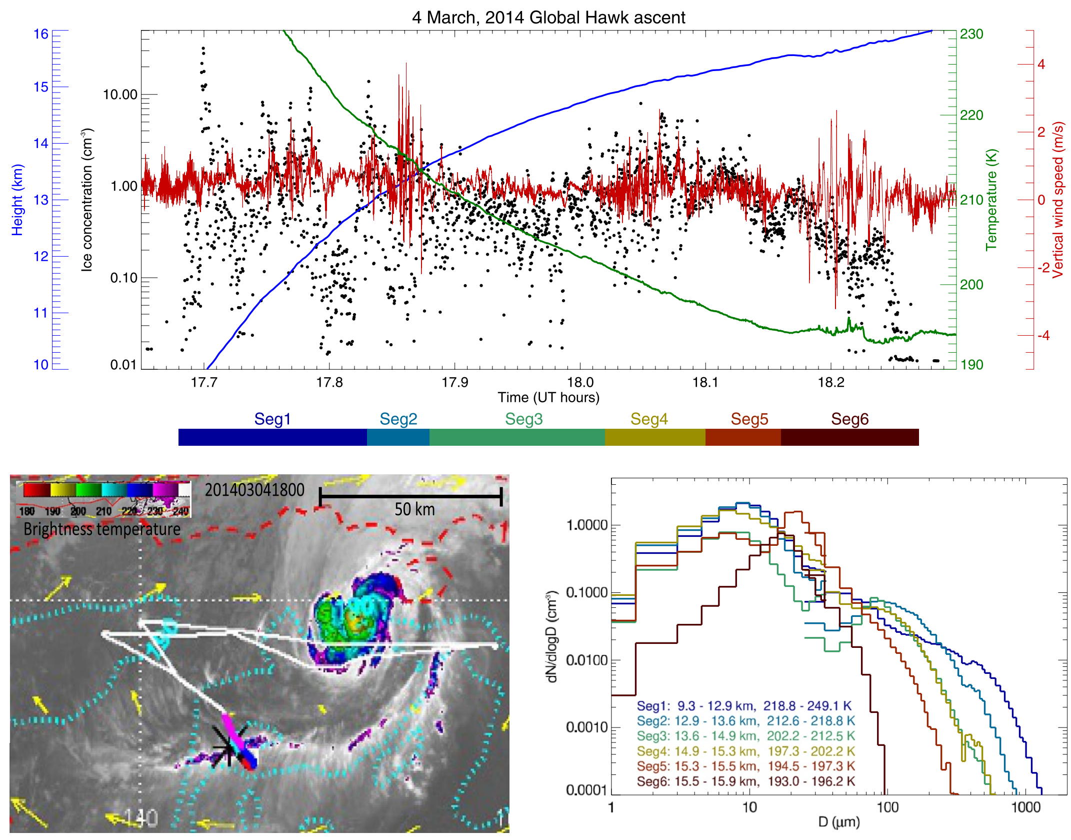

Figure 1. Top panel: Time series of Airborne Tropical Tropopause Experiment (ATTREX) in situ measurements during the 4 March 2014 Global Hawk ascent through a band of developing convection emanating from tropical cyclone Faxai: aircraft altitude (blue), temperature (green), vertical wind speed (red), and ice concentration (black dots). Lower left: satellite image showing the flight segment (magenta) through the band of convection from Faxai. Lower right: Size distributions averaged over the segments indicated under the top-panel time series plot. The height and temperature ranges for the segments are given in the legend.

and POSIDON aircraft payloads included the Meteorological Measurement System that measured temperature, pressure, and vertical wind speed (Scott et al., 1990).

On the 4 March 2014 ATTREX flight, the initial climbout of the Global Hawk passed through a developing band of deep convection emanating from tropical cyclone Faxai northwest of Guam. Abundant ice crystals (up to ≈10 cm^{-3}) were sampled through a deep layer extending from about 10 to 15.5 km (Figure 1). The measured ice water content (IWC) exceeded 50 ppmv in multiple layers during the ascent. Patches of vertical wind speed as high as 3 m s^{-1} were observed, consistent with the active dynamics associated with the convection.

The bottom right panel of Figure 1 shows ice crystal size distributions measured during the ascent averaged over height ranges. Through most of the depth of the convection, abundant small ice crystals ($D < 20$ μm) were present. The concentration and size of large ice crystals decreased with increasing height in the cloud, as expected from the effects of sedimentation. Crystals smaller than 20 μm were depleted at the top of the cloud. Note that we are not interpreting the aircraft ascent through the convective system as a coherent sampling of a rising column. Since the aircraft primarily travels horizontally even during climbout, different parts of the convective system were necessarily sampled at different altitudes. Nonetheless, the vertical dependence of ice crystal size distributions is quite systematic, at least for the larger ice crystals.

During the POSIDON flight on 15 October 2016, the WB-57 ascended through a band of convection and fresh anvil cirrus at the edges of typhoon Haima southwest of Guam (Figure 2). In this case, the ice crystal number concentrations were as large as 8 cm^{-3}. Vertical wind speeds approached 4 m s^{-1} in the most active patch (Seg1). The ice crystal size distribution in this segment was broad, including abundant small crystals and large crystals with maximum dimensions approaching 1 mm. In the adjacent flight segment (Seg2), the ice concentrations were

AGU ADVANCING EARTH AND SPACE SCIENCES

Journal of Geophysical Research: Atmospheres

10.1029/2023JD039887

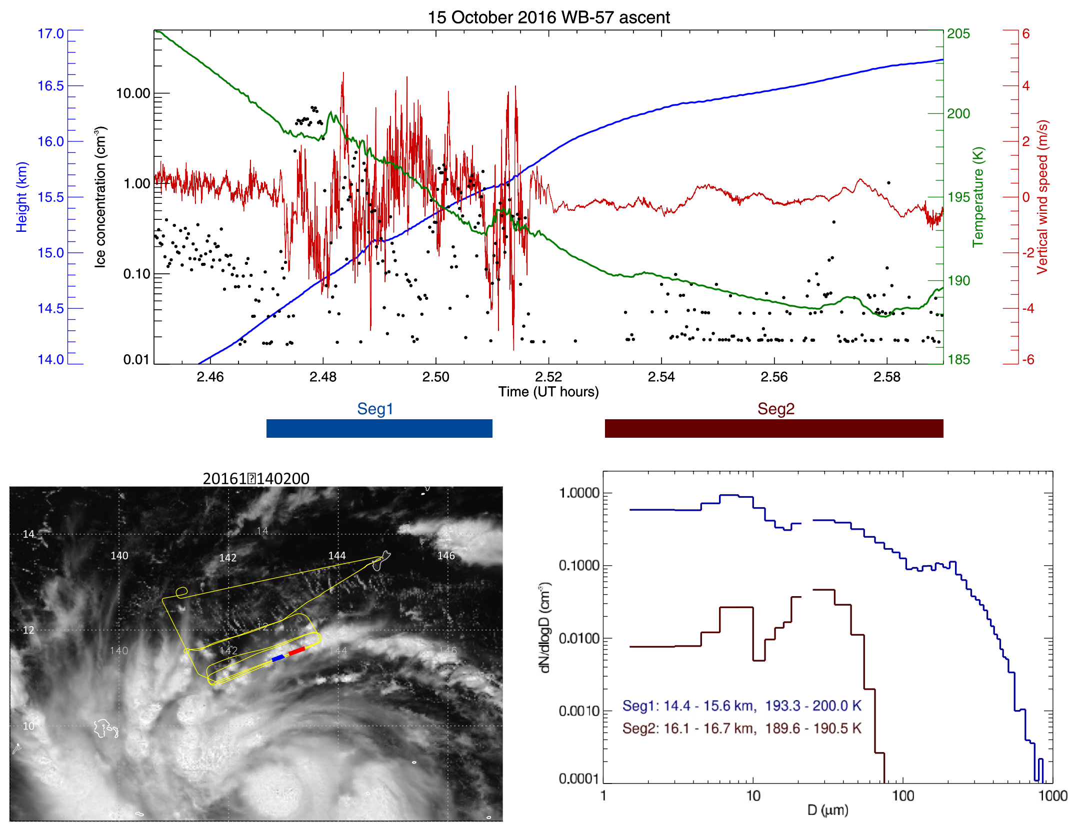

Figure 2. Top panel: Time series of Pacific Oxidants, Sulfur, Ice, Dehydration, and cONvection (POSIDON) in situ measurements during the WB-57 transect through a band of convection emanating from tropical cyclone Haima: aircraft altitude (blue), temperature (green), vertical wind speed (red), and ice concentration (black dots). Lower left: satellite image showing the flight segment along a band of convection. Lower right: Size distributions averaged over the two different flight segments shown underneath the time series plot in the top panel.

generally less than 100 L^{-1}, with relatively few small crystals and no ice crystals with maximum dimensions larger than ∼70 μm.

The 10 August 2016 StratoClim Geophysica flight sampled strong, active convection near the tropopause over southern Asia during the monsoon season (Figure 3). Ice concentrations of 1–10 cm^{-3} were measured at altitudes of 16–17 km. IWCs as high as 3,000 ppmv were observed, consistent with strong, active convection (Lamraoui et al., 2023). As in the ATTREX and POSIDON cases, the ice crystal size distributions in the convective segments (Seg1 and Seg3) were broad with abundant small crystals as well as crystals up to 1,000 μm. In a patch of cirrus between the active convection segments (Seg2), relatively few small crystals were measured (particularly in the 3–10 μm size range), and no crystals with maximum dimensions larger than 100 μm were detected. The observed microphysical properties of active convection and anvil cirrus from the three campaigns are qualitatively consistent: The active convection contains high concentrations of small ice crystals as well as some large aggregates. In the aged anvil cirrus, both small and large crystals are generally absent.

3. Model Description

Our focus here is on the impacts of wave-driven temperature fluctuations on the evolution of anvil cirrus microphysical properties. For this purpose, we use a one-dimensional model framework, with ice microphysics simulated using the Community Aerosol and Radiation Model for Atmospheres (CARMA) bin microphysics model (Bardeen et al., 2008; Jensen et al., 2002; Toon et al., 1988). We use 85 ice crystal size bins, spanning a size range of 0.3 μm–3.7 mm; the ratio of particle volumes in successive bins is 1.4. For simplicity, we assume the ice crystals are equivalent-mass spheres. The maximum dimensions of ice crystals with complex habits could be considerably larger than the diameters of equivalent-mass spheres assumed here, and the spherical ice crystals

10.1029/2023JD039887

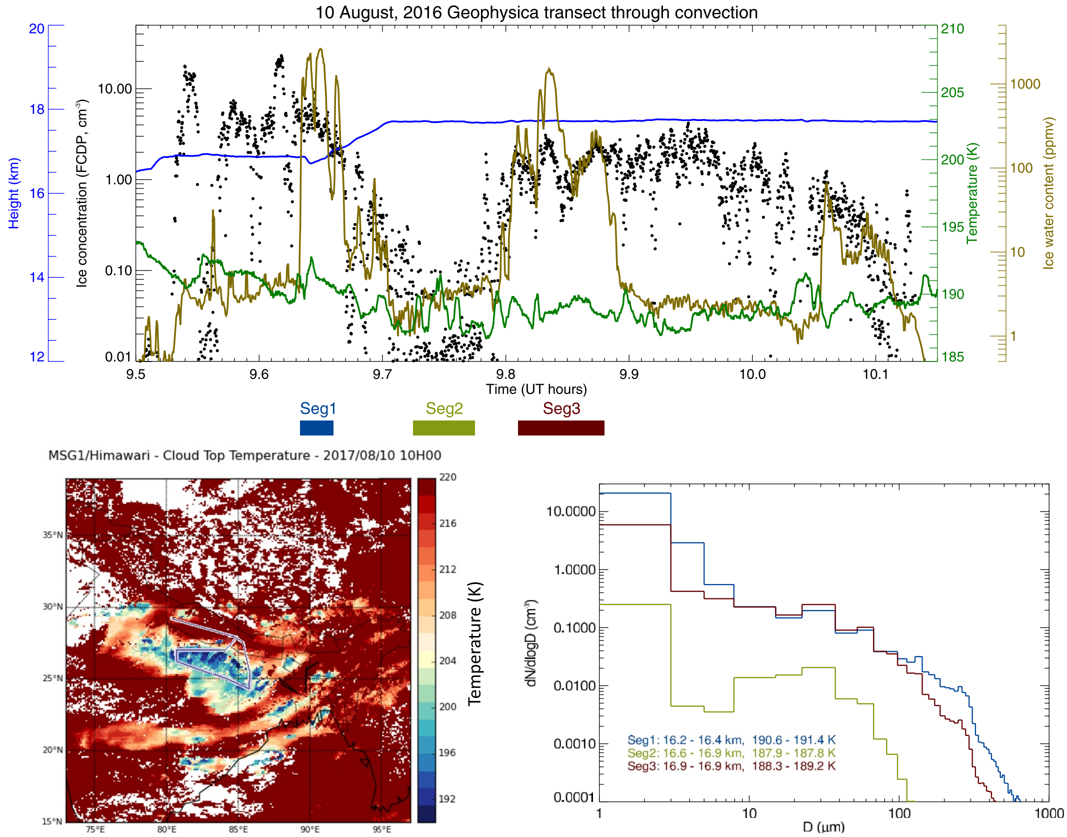

Figure 3. Top panel: Time series of StratoClim in situ measurements during the 10 August 2016 Geophysica transit through deep convection and anvil cirrus near the tropopause: aircraft altitude (blue), temperature (green), ice water content (red), and ice concentration (black dots). Lower left: satellite image showing the flight segment (black line) through the active convection. Lower right: Size distributions averaged over different time segments. The segment times are indicated under the time series plot.

will fall faster than non-spherical ice crystals. The dependence of sedimentation loss of large ice crystals from anvil cirrus on habit was explored in detail by Jensen et al. (2018). The focus here is on the impacts of waves and the Kelvin effect on small ice crystals and the total ice concentration. The model vertical domain is either 13–18 km or 9–14 km, depending on whether we are simulating high or low tropical anvil cirrus. The vertical grid spacing is 20 m. We ran a few test simulations with 10 m vertical resolution, and the results were essentially unchanged. We initialize the model with a 2-km thick cloud (either 15.5–17.5 km or 11.5–13.5 km). The high anvil case corresponds to an extreme convective system producing an anvil up against the tropical tropopause. The low anvil case corresponds to the typical tropical convection detrainment level. Based on the measurements presented in Section 2, we initialize the anvil with abundant ice crystals and a broad ice crystal size distribution. For the high/cold anvil case, we use a log-normal distribution with a total concentration of $N_i = 2$ cm^{-3}, a mode radius of $r_m = 3$ μm, and a geometric standard deviation of $\sigma = 3$. Since lower anvils generally have larger ice crystals, we use $\sigma = 3.5$ for the 11.5–13.5 km anvil simulations. The temperature profile is based on wintertime soundings from Guam. With this temperature profile, the temperature ranges for the high and low anvil cases are 188.6–202 K and 217.6–231.4 K, respectively. We initialize the model with an ice saturation ratio of unity within the cloud. Below the cloud, we maintain a saturation ratio near zero such that ice crystals rapidly sublimate when they fall below the initial cloud base. Simulated physical processes include ice deposition growth, sublimation, and sedimentation. The simulations are run for 24 hr.

We note that this model framework omits a number of physical processes that can affect anvil evolution. Mesoscale circulations, small-scale convection, and turbulence driven by cloud radiative heating can affect the structure and microphysical properties of aging anvil cirrus (Gasparini et al., 2019). It is likely that long-lived anvils are maintained by synoptic-scale meteorological support (upward motion). The internal anvil dynamics and

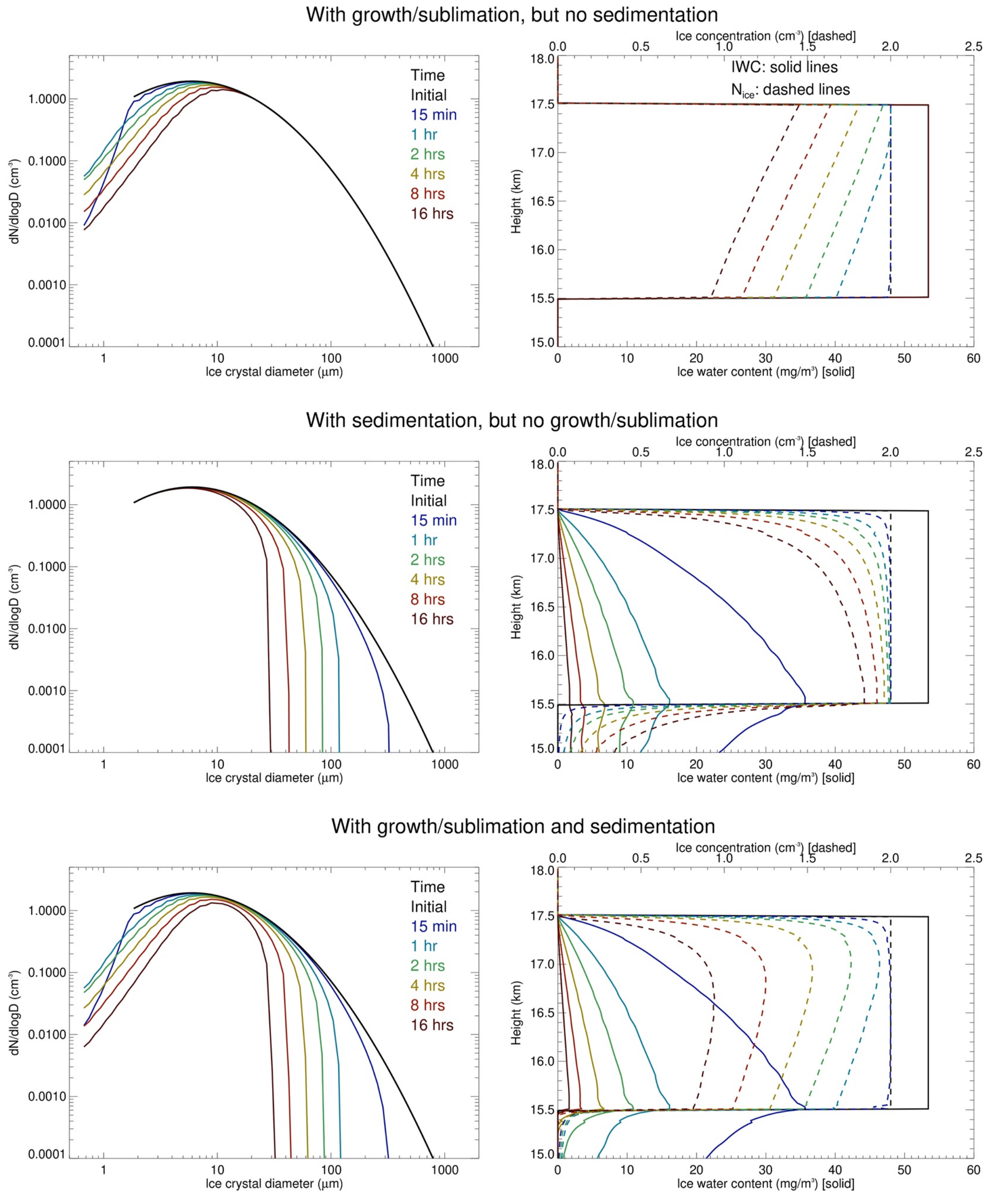

Figure 4. Results from the high/cold anvil simulations with no wave-driven temperature perturbations. Left panels: evolution of ice crystal size distribution averaged over cloud depth (15.5–17.5 km). Times corresponding to the different colored curves are indicated in the legend. Right panels: vertical profiles of ice water content (solid) and ice concentration (dashed) Top row: no ice crystal sedimentation included; middle row: no ice growth/sublimation included; bottom row: both sedimentation and growth/sublimation included.

large-scale ascent could potentially drive supersaturation and ice nucleation, particularly if effective heterogeneous ice nuclei are available. Wind shear will stretch and thin the anvils over time. The simple approach used here was chosen to isolate the wave effects on the evolution of anvil microphysical properties.

4. Evolution of Anvil Without Waves

We start by examining the evolution of anvil without wave-driven temperature perturbations. Figure 4 shows the evolution of the cloud-averaged ice crystal size distribution and the vertical profiles of ice concentration and IWC

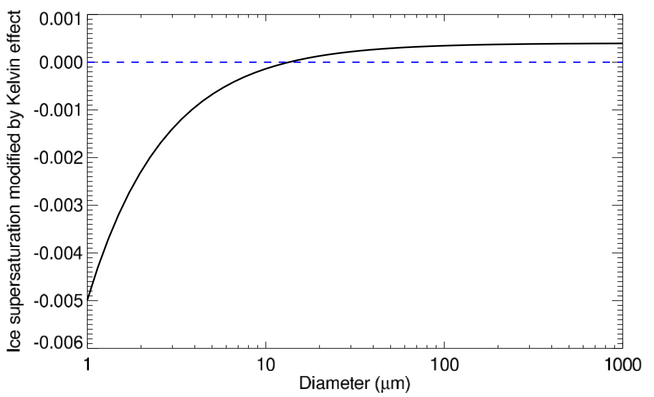

Figure 5. The ice saturation ratio modified by the Kelvin effect is plotted versus ice crystal diameter. Shortly after the simulation begins, a quasi-steady state is established with slight supersaturation for large (low curvature) ice crystals and effective subsaturation for small (high curvature) ice crystals, resulting in mass transfer from small to large crystals.

for the high/cold anvil case. Results are shown for simulations without sedimentation (isolating the effects of deposition growth and sublimation), with no growth (isolating the effects of sedimentation), and with both processes included.

Without sedimentation included and with the initial ice saturation ratio set to unity, one might expect the cloud to be static, with no change in the ice concentrations or size distribution. However, the Kelvin effect (higher saturation vapor pressure over curved surfaces than over a planar surface) means the smallest crystals have a higher saturation vapor pressure and lower effective saturation ratio than larger crystals. Specifically, the Kelvin term that modifies the saturation vapor pressure is given by

$$\frac{p_{sat,i,eff}}{p_{sat,i}} \equiv a_k = \exp\left(\frac{2\sigma_{i/a}}{R_w T \rho_i r_i}\right) \tag{1}$$

where $p_{sat,i,eff}$ is the effective saturation vapor pressure over a spherical ice crystal with radius r_i, $p_{sat,i}$ is the saturation vapor pressure over a planar ice surface, $\sigma_{i/a}$ is the surface energy of the ice/air interface, R_w is the specific gas constant for water vapor, T is the temperature, and ρ_i is the ice density. As a result of the Kelvin effect, the system quickly establishes an approximate steady state with slight supersaturation for crystals larger than ∼10 μm and significant subsaturation for smaller ice crystals (Figure 5). The supersaturation dependence on ice crystal size results in mass transfer from small to large ice crystals. As shown on the top right panel of Figure 4, the IWC is exactly conserved without sedimentation, but the ice concentration decreases as a result of complete sublimation of small ice crystals. The ice concentration reduction is more pronounced at lower heights in the anvil because the deposition growth/sublimation rates are faster at higher temperatures.

If we shut off deposition growth/sublimation and only include sedimentation (middle row of panels in Figure 4), the large ice crystals rapidly fall out of the anvil, resulting in rapid reduction in IWC, particularly in the upper part of the cloud (e.g., after only 15 min, the column-integrated ice mass has decreased more than a factor of 2.). Ice crystals smaller than about 10 μm are unaffected. The ice concentration is reduced slightly by the sedimentation of large crystals out of the upper part of the cloud.

If both growth/sublimation and sedimentation are included (bottom row of panels in Figure 4), then both small and large ice crystals are lost, leaving a narrow ice crystal size distribution composed primarily of ice crystals with diameters ranging from about 5 to 20 μm (Kärcher et al., 2023). The IWC is dominated by sedimentation and decreases rapidly, as noted above. The ice concentration decreases relatively slowly, with about a factor of two reduction after ∼8 hr.

Figure 6 shows the results of equivalent simulations for a lower (11.5–13.5 km), warmer anvil. The higher temperatures in the lower anvil mean deposition growth and sublimation rates are much faster. Specifically, growth/sublimation rates are about a factor of 25 faster at the low anvil mid-cloud temperature of 225.6 K than at the high anvil mid-cloud temperature of 196.6 K. As a result, the loss of small ice crystals resulting from the Kelvin effect is much faster for the low anvil. Even without sedimentation (top panels in Figure 6), ice concentrations are reduced a factor of 2 in about 1.5 hr. Seeley et al. (2019) also noted that higher anvil cirrus should last longer than lower anvil cirrus because sublimation is faster at warmer temperatures. Sedimentation rates are slightly slower for the lower anvil (as a result of higher atmospheric density), but overall, the reductions in ice mass and ice concentration resulting from sedimentation alone are similar for the low and high anvils. With both growth/sublimation and sedimentation acting, the decrease in ice concentration is more rapid for the low anvil than for the high anvil (bottom panels in Figures 4 and 6). As a result, in the lower/warmer anvil the ice size distribution narrows faster than in the higher/colder anvil.

5. Impact of Monochromatic Gravity Waves

Next, we examine the impact of temperature variations driven by coherent, monochromatic high-frequency waves. As noted above, modeling and observational studies have shown that deep convection can generate coherent waves, and situations with approximately monochromatic waves are sometimes observed in the tropical upper

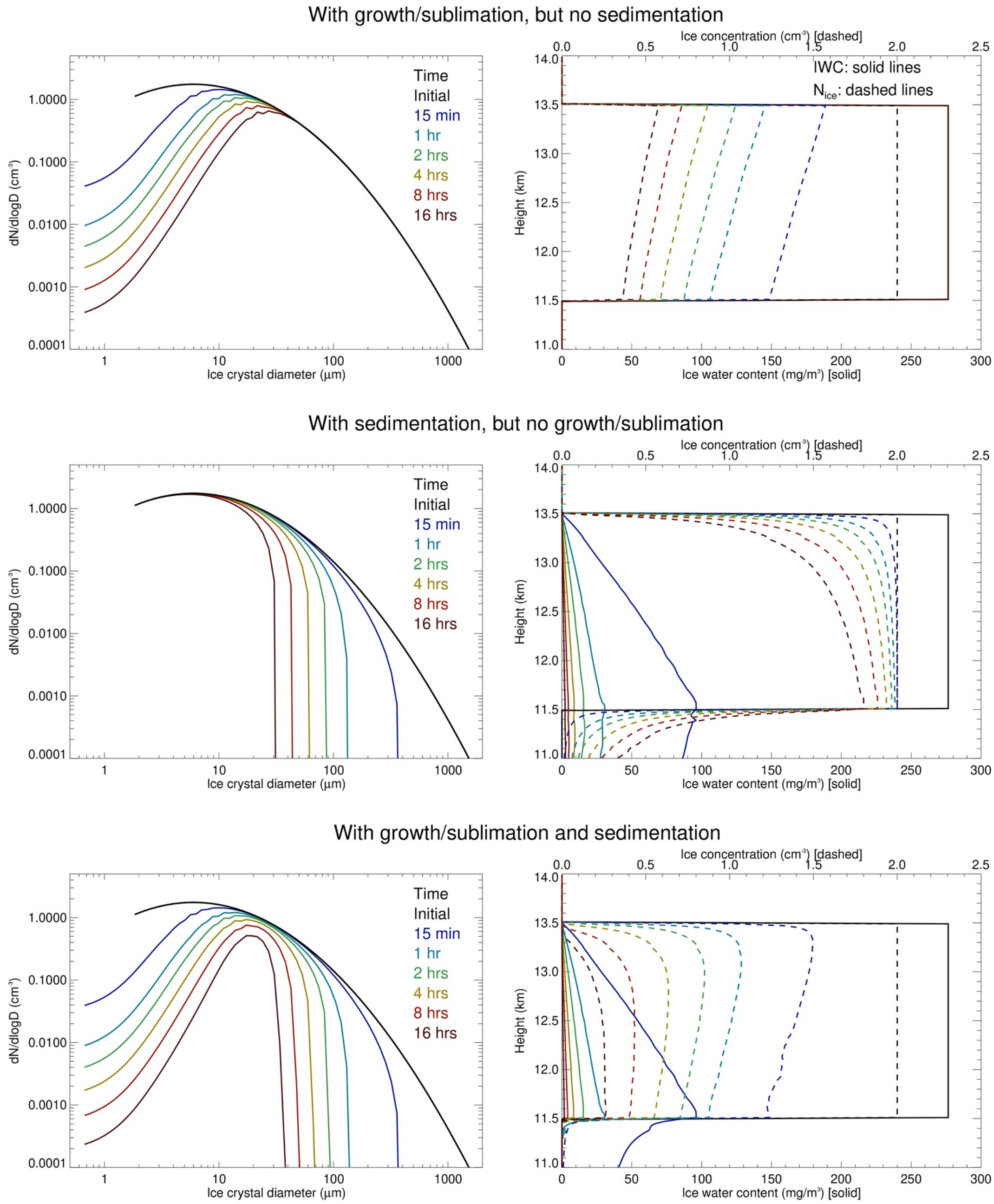

Figure 6. Same as Figure 4, but results from the low/warm anvil (11.5–13.5 km) are shown.

troposphere (Atlas & Bretherton, 2023; Podglajen et al., 2017). Although monochromatic waves are not typical in the upper troposphere, examining their impact on anvil microphysics is nonetheless instructive.

We begin by using a simple sinusoidal temperature oscillation with a period of 60 min and an amplitude of 0.25 K. Figure 7 shows the evolution of the ice crystal size distribution with and without waves at a height of 16.5 km, which is in the middle of the high/cold anvil. Small ice crystals sublimate rapidly in the warm phases of the wave, and larger crystals grow (see Section 6). The net result is an accelerated loss of ice crystals smaller than ∼10 μm compared to the simulation with no waves. The wave has little impact on IWC evolution because the contribution of small ice crystals to the ice mass is negligible.

Figure 8 shows the evolution of temperature, cloud fields, and supersaturation at 16.5 km in the monochromatic wave simulation. In the warming phases of the wave, the supersaturation decreases to zero, but because of the

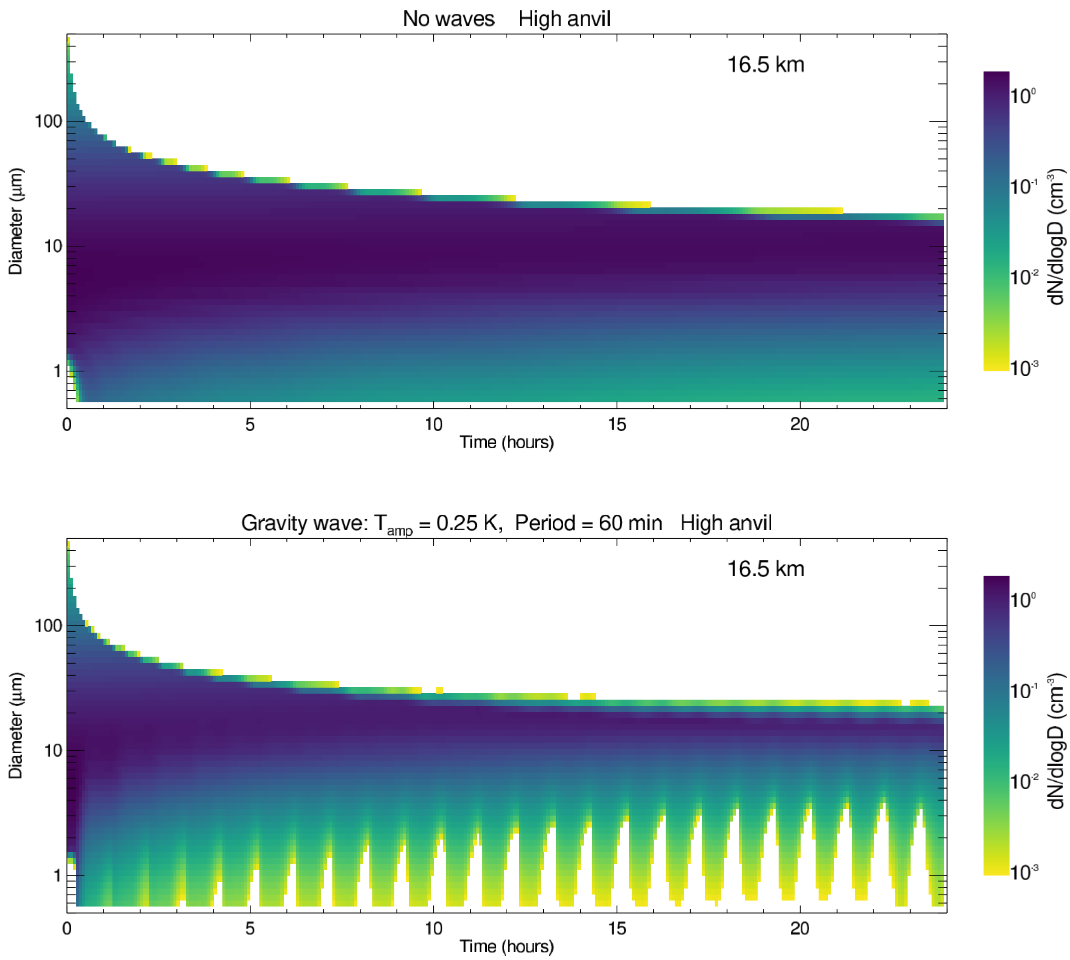

Figure 7. Contours of ice concentration are plotted versus time and ice crystal diameter. Results are shown at an altitude of 16.5 km, which is the middle of the cold/high anvil. Top panel: no waves; bottom panel: monochromatic wave with a temperature amplitude of 0.25 K and a period of 60 min. In the bottom panel, the extensions of the size distribution to sizes smaller than a few microns occur in the warming phases of the wave when sublimation occurs.

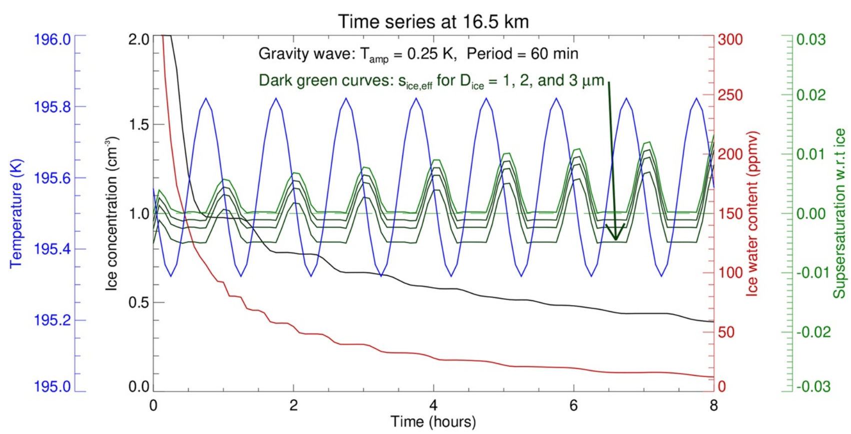

Figure 8. The time evolution of Temperature (blue), ice concentration (black), ice water content (red), and supersaturation with respect to ice (green) at the mid-cloud altitude (16.5 km) are plotted versus time for the high/cold anvil case with a monochromatic wave (T_{amp} = 0.25 K, period = 60 min). Only the first 8 hr of the simulation are shown. The dark green curves show the supersaturation modified by the Kelvin effect for ice diameters of 1, 2, and 3 μm.

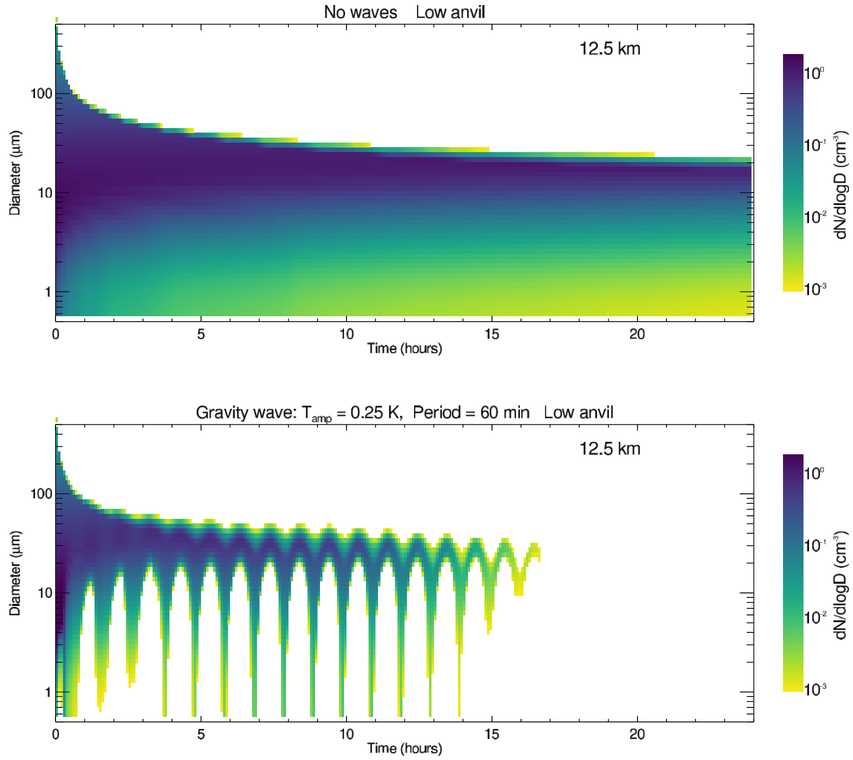

Figure 9. Same as Figure 7, but results are shown for low/warm anvil simulations.

Kelvin effect, small ice crystal sublimate rapidly, resulting in reduction of ice concentration. The sublimation of small crystals also prevents the saturation ratio from dropping below zero, which prevents sublimation of crystals large enough for the Kelvin effect to be negligible. As shown in Section 6, growth of crystals with initial diameters in the 4–10 μm range in the cooling phases of the wave also decreases the concentration of small crystals. The growth of crystals in the cooling phases of the wave depletes the vapor, limiting the peak supersaturation. As the ice mass decreases over time due to sedimentation, peak supersaturations in the cooling phases increase.

Figure 9 shows the impact of the wave on the low/warm anvil ice crystal size distribution. In this case, the wave impact is even more dramatic because ice growth and sublimation rates are much more rapid at the warmer temperature of the low anvil. The wave essentially destroys the cloud after several hours. The temperature oscillations drive sublimation of crystals smaller than about 5 μm, somewhat larger crystals rapidly grow, and sedimentation still removes ice crystals larger than 20–30 μm. As a result, with the low, warm anvil, the size range of ice crystals that are not removed by sublimation or sedimentation becomes very narrow, resulting in accelerated destruction of the cloud.

Figure 10 shows the sensitivity of anvil ice concentration and IWC to wave amplitude. Not surprisingly, waves with larger temperature amplitudes reduce the ice concentration more rapidly, but even relatively low-amplitude waves decrease the ice concentration significantly. In the low, warm anvil case with a wave amplitude of only 0.05 K, the ice concentrations are reduced by an order of magnitude in about 6 hr. In the cold anvil case, waves have little impact on the IWC evolution, but in the warm case waves are driving removal of most of the ice crystals, and ice mass reduction is accelerated. With relatively large wave amplitudes in the warm anvil simulation, large oscillations in IWC are driven by the temperature oscillations. The impact of waves also increases with decreasing wave period (not shown) because shorter period waves drive faster heating/cooling rates.

The most rapid reduction in ice concentration occurs during the first hour of the simulations with waves. This initial drop in ice concentration is primarily driven by sublimation of ice crystals small enough for the Kelvin effect to significantly raise the saturation vapor pressure. Also shown in Figure 10 are results from simulations with a wave amplitude of 0.25 K, but with the Kelvin effect not included ($a_k = 1$). For the high/cold anvil, excluding the Kelvin effect results in a slow decrease in ice concentration. In the low/warm anvil case, the wave rapidly

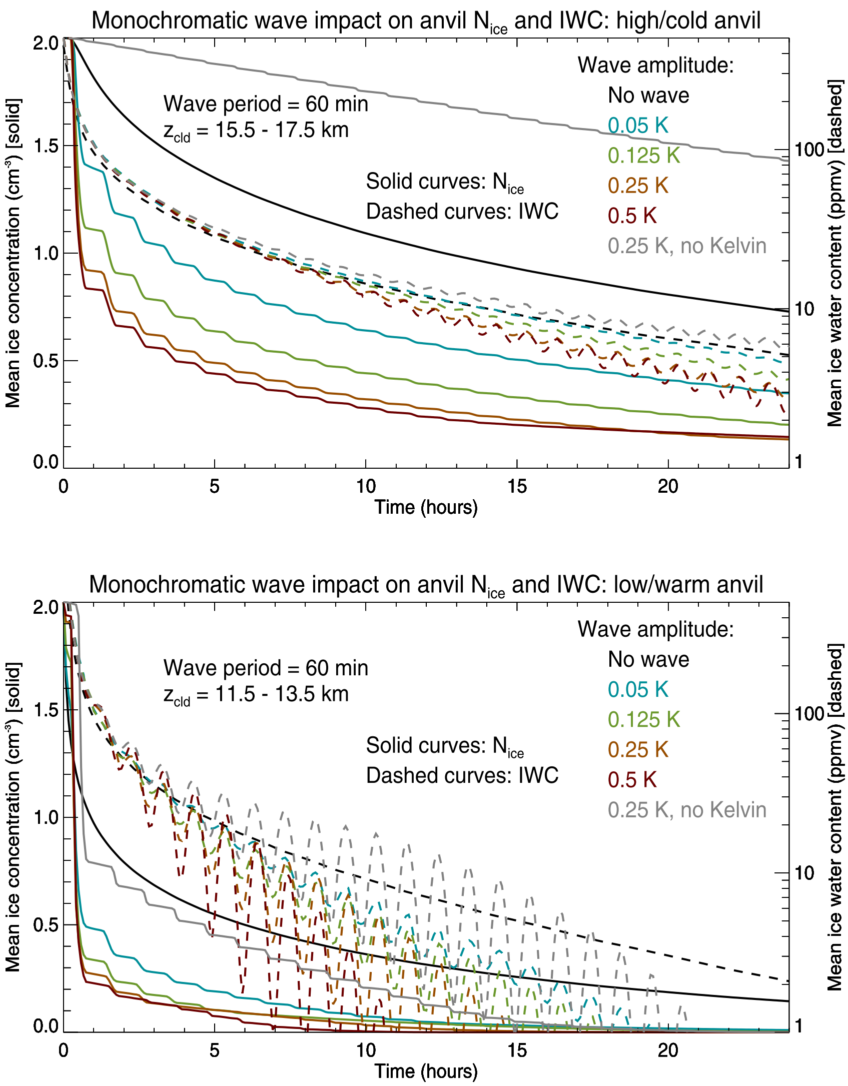

Figure 10. The vertically-averaged ice concentration (solid) and ice water content (dashed) are shown versus time for the simulation with no waves (black curves) and simulations with different wave amplitudes (see legend). The gray curve shows results from a simulation with the 0.25 K wave but no Kelvin effect included. Top panel: results for high, cold anvil; bottom panel: results for low, warm anvil.

decreases the ice concentration even without the Kelvin effect included. Again, the stronger sensitivity to waves in the low anvil case is caused by the faster sublimation rates at higher temperatures.

6. Lagrangian Tracking of Individual Ice Crystals

With the purely Eulerian modeling approach used to this point, wherein ice concentrations are tracked in diameter and height bins, it is not possible to determine the evolution of individual ice crystal sizes. For this purpose, we have added Lagrangian tracking of individual ice crystals. At the beginning of each simulation, we initialize 70 individual Lagrangian ice crystals in the upper parts of the anvils (17 km for the high anvil and 13 km for the low anvil). The initial sizes of the Lagrangian ice crystals range from 0.5 to 65 μm. At each time step, we interpolate the deposition growth/sublimation rates and fallspeeds from the Eulerian size and height grids to the current size and height of each Lagrangian ice crystal. Then we update the sizes and heights of the crystals.

Figure 11 shows the evolution of crystal diameters in simulations of the high anvil with monochromatic waves (T_{amp} = 0.25 K, period = 60 min). Results are shown with and without the Kelvin effect and ice sedimentation included. Without the Kelvin effect, ice crystals that start smaller than about 1 μm sublimate completely in the

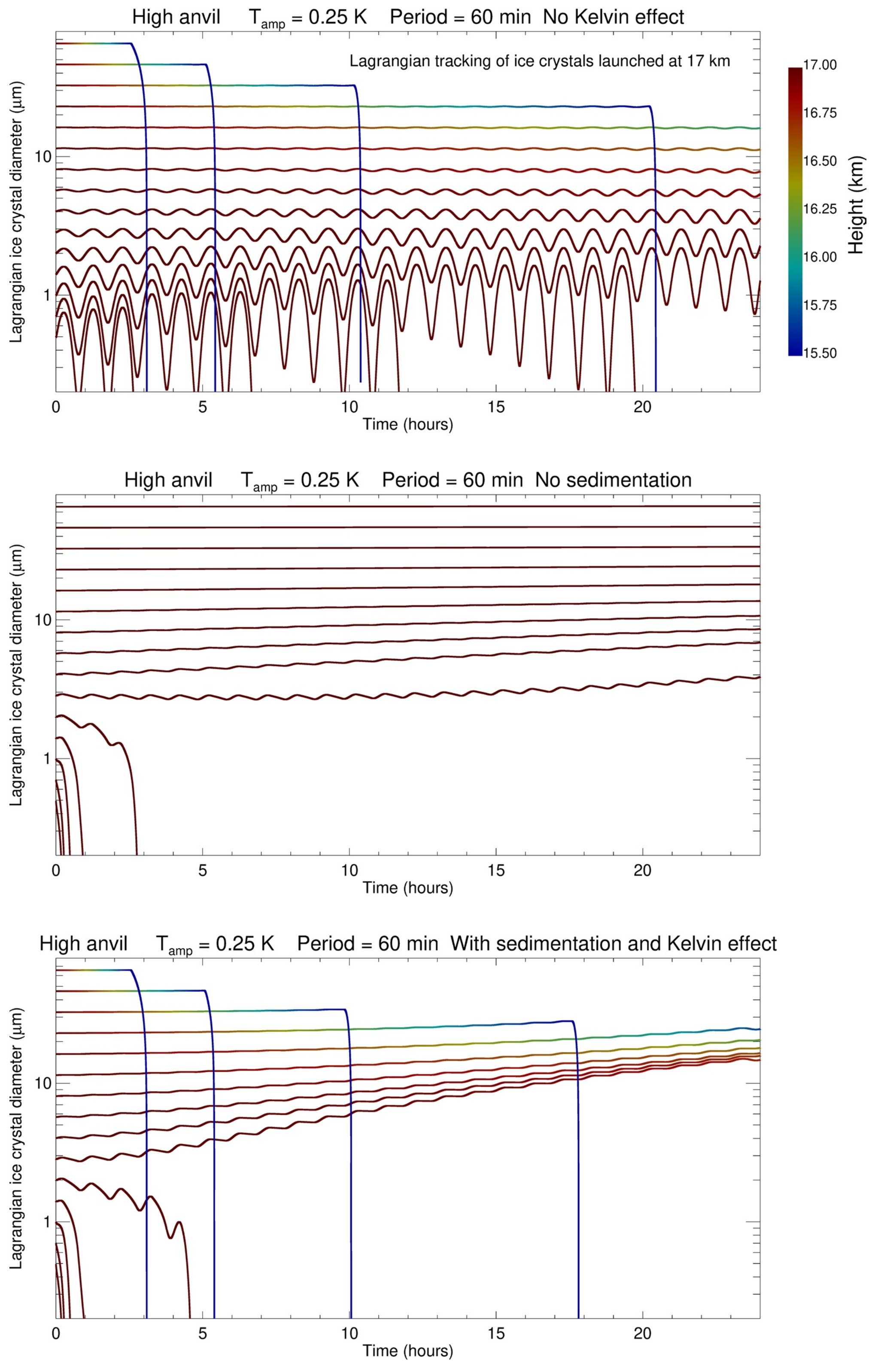

Figure 11. The evolution of individual ice crystal diameters are plotted versus time. The ice crystals are initialized at 17 km, and the height versus time for each crystal is indicated by the colors along the curves. Results are shown for the high/cold anvil case with a monochromatic wave having a temperature amplitude of 0.25 K and a phase of 60 min. Top panel: No Kelvin effect included ($a_k = 1$); middle panel: no sedimentation; bottom panel: both sedimentation and the Kelvin effect included.

warm phase of the wave, but otherwise, the ice crystal sizes just oscillate with the temperature/supersaturation oscillation, with no significant net change in size. Ice crystals larger than about 20 μm sediment into the dry sub-cloud air and sublimate.

With the Kelvin effect included, but no sedimentation (middle panel of Figure 11), the large ice crystals stay at their original heights, and they maintain the ice saturation ratio near unity, such that growth of ice crystals is limited even though the smallest crystals sublimate. With both the Kelvin effect and sedimentation included (bottom panel), the largest ice crystals rapidly sediment out, and ice crystals with initial sizes ranging from about 2 to 10 μm grow to about 20 μm. The sedimentation loss of the largest crystals allows larger supersaturations to build up in the cooling phases of the wave, which essentially allows the mid-sized crystals to grow larger than they could in the simulation without sedimentation.

Figure 12 shows the equivalent Lagrangian ice crystal tracking results for the low/warm anvil case. In the simulation with the Kelvin effect excluded, ice crystals with initial diameters smaller than ≈10 μm completely sublimate within the first couple of wave cycles. Ice crystals larger than a few 10 s of microns still sediment out of the cloud within a few hours, leaving a narrow size range of ice crystals that survive.

With the Kelvin effect included, but no sedimentation, ice crystals with initial diameters of about 4–20 μm grow to ≃30 μm within several hours. With both the Kelvin effect and sedimentation included, the 4–10 μm crystals rapidly grow to about 20 μm, but larger crystals are lost to sedimentation, again leaving a narrow range of ice crystals that survive, and complete destruction of the cloud in less than 16 hr.

As discussed in Section 2, in situ measurements show that ice crystal habits in anvil cirrus rapidly transition from primarily pristines, irregulars, and aggregates in the fresh convective outflow to predominantly bullet rosettes in the aged anvils, and the bullet rosette habit is an indication of in situ growth of the ice crystals at upper tropospheric conditions. The simulations presented here suggest that the interaction between wave-driven temperature oscillations, deposition growth/sublimation with the Kelvin effect, and ice sedimentation results in growth of mid-sized ice crystals, which could explain the observed transition to bullet rosette habits.

We note also that laboratory results indicate that significant supersaturations are required for growth of bullet rosettes (Bailey & Hallett, 2004). Gravity wave temperature fluctuations are perhaps the leading mechanism for generating the observed substantial supersaturations within cirrus clouds (Krämer et al., 2009). This requirement represents another mechanism by which gravity-wave generated temperature fluctuations may explain the transition to bullet rosettes in evolving anvil cirrus.

7. Impact of Stochastic, Mesoscale Temperature Fluctuations

As noted above, numerous measurements have shown that MTFs are present much of the time in the tropical upper troposphere (Atlas & Bretherton, 2023; Kärcher & Podglajen, 2019). These fluctuations are likely caused by superposition of gravity waves from different sources with different frequencies and phases. Podglajen et al. (2016) characterized these fluctuations based on long-duration, approximately Lagrangian superpressure balloon measurements. In the deep tropics, the distributions of vertical wind perturbations is close to a Laplace (double exponential) distribution. Kärcher and Podglajen (2019) and Podglajen et al. (2016) developed probabilistic models describing the MTF. We note that previous studies have directly used the super-pressure balloon temperature time series for simulations of temperature fluctuation influence on TTL cirrus (Corcos et al., 2023; Dinh et al., 2016). Whereas we are using ensembles of the essentially equivalent synthetic temperature time series. We use the microphysical model described above to investigate the influence of MTF on evolution of ice microphysics in anvil cirrus. As noted above, we are not addressing the impact of waves on ice nucleation.

The approach developed by Kärcher and Podglajen (2019) for generating MTF time series involves randomly selecting vertical wind perturbations from a Laplace distribution. The procedure includes choosing a vertical wind variance, generating a vertical wind autocorrelated perturbation time series by selecting values randomly from the Laplace distribution, and then generating the corresponding temperature perturbation time series. As a baseline case, we chose a vertical wind standard deviation of 15 cm s^{-1}, which is typical of the observed vertical wind speed amplitudes (Kärcher & Podglajen, 2019). Since the vertical wavelengths of high-frequency gravity waves are generally larger than the vertical depth of the anvils simulated here (2 km) (Vincent & Alexander, 2000), we assume the temperature fluctuations are vertically coherent. In other words, we apply the same temperature perturbations to all vertical levels in the model.

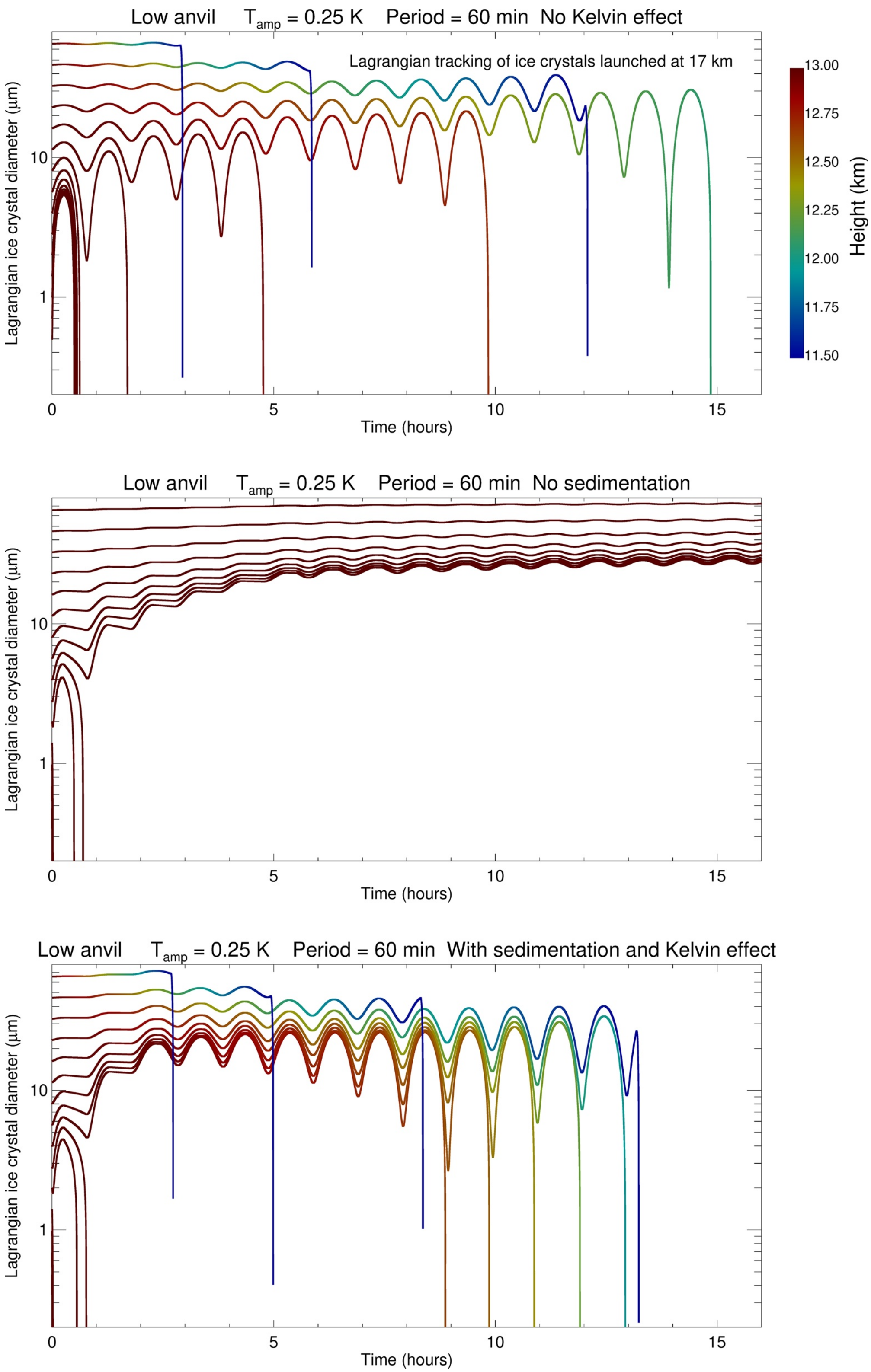

Figure 12. Same as Figure 11, except for the low/warm anvil case. Note that we are only showing the first 16 hr of cloud evolution here.

10.1029/2023JD039887

The MTF time series generated with this approach presumably represent a superposition of temperature fluctuations from waves with different frequencies, phases, and amplitudes. Wave frequencies ranging from the Coriolis to the Brunt-Vaisala frequency may be included. However, we are only running 24-hr simulations, thus we are implicitly not including longer period waves (such as Kelvin waves). We believe the majority of the microphysical impact of the MTF is associated with relatively high-frequency waves (periods ranging from about 15 min to hours).

This approach basically generates temperature perturbations that represent wave-driven MTFs sufficiently far away from the deep convective source (background MTFs). Corcos et al. (2021) showed that MTFs level off to background conditions more than several 100 km away from active deep convective cores. Closer to the convective source, temperature variances can be larger, more transient, and not straightforward to model. Therefore, we employ background MTFs as, compared to a monochromatic wave, a more realistic, observation-based variant to study wave effects on anvil microphysics.

Given the random element in this approach, we need to run ensembles of simulations to determine the statistical mean evolution of the anvil, as well as the variability amongst different realizations. For each set of assumed initial conditions and physical processes, we run ensembles of 400 simulations using unique realizations of MTF temperature perturbation time series. The MTF temperature variance averaged across all time series in the ensemble was 1 K^2.

An example of the high/cold anvil evolution for a particular MTF time series is shown in Figure 13. The temperature increases by ~2 K during the first 2 hr, driving rapid reduction in ice concentration. The ice concentration at 16.5 km has decreased to a few hundred per liter by about 6 hr. After about 7 hr, the temperature decreases for several hours, and the ice concentration remains roughly constant. The remaining ice crystals sublimate near the end of the simulation when the temperature rises well above the initial value. As in the monochromatic wave simulations, the initial rapid reduction of IWC is primarily caused by sedimentation of large crystals, but sublimation of small ice crystals contributes to some degree, particularly toward the end of the simulations.

The mean ice concentration and mean IWC in the ensemble of 400 anvil simulations with MTF are shown in Figure 14. With MTF included, the high/cold anvil ice concentrations decrease rapidly in the first few hours, quickly decreasing to concentrations about a factor of 3 lower than in the simulation with no MTF. The spread between ice concentrations with different MTF realizations is less than a factor of 2. The IWC evolution in the high anvil is only slightly affected by MTF, at least in the ensemble mean. Some ensemble members had rapid reductions in IWC after about 15 hr.

The mean ice concentration and mean IWC for the low/warm anvil simulations with MTF are shown in the right panels of Figure 14. As in the case with monochromatic waves, the temperature fluctuations have a much stronger impact on the low anvil because of the higher temperatures and faster process rates. In this case, the ice concentrations decrease rapidly, dropping to values less than 20 L^{-1} within 2–10 hr. Likewise, the IWC decrease with time is strongly accelerated after about 2 hr in the low anvil simulations with MTF. The anvils essentially disappear no later than about 10 hr into the simulations.

The amplitudes of upper tropospheric MTF are quite variable in space and time. In particular, we are interested in the intrinsic (Lagrangian) wave parameters since we're essentially tracking the anvil as it is advected downwind. Many of the observational techniques only provide the Eulerian wave parameters. Kärcher and Podglajen (2019) showed that the MTF amplitudes can differ in the Eulerian and Lagrangian reference frames. Figure 15 summarizes the sensitivity of ice concentration evolution to doubling or halving MTF amplitudes. The difference are relatively small compared to the differences between simulations with no waves and those including MTF. For the high/cold anvil case, decreasing MTF amplitudes by a factor of 2 has little impact, but increasing the amplitudes by a factor of 2 significantly accelerates ice loss toward the end of the simulations. For the low/warm anvil case, the factor of 4 range of MTF amplitudes corresponds about a factor of 2 range in the anvil lifetime.

Lastly, Figure 16 shows the frequency distributions of ice concentration from simulations with/without MTF superimposed and with/without the Kelvin effect included. For the high anvil case at 8–12 hr simulation time, including MTF reduces the ice concentration by about a factor of 3 compared to the simulation with no waves. Without the Kelvin effect, the ice concentration distribution is simply broadened, and the ice concentrations are not reduced overall.

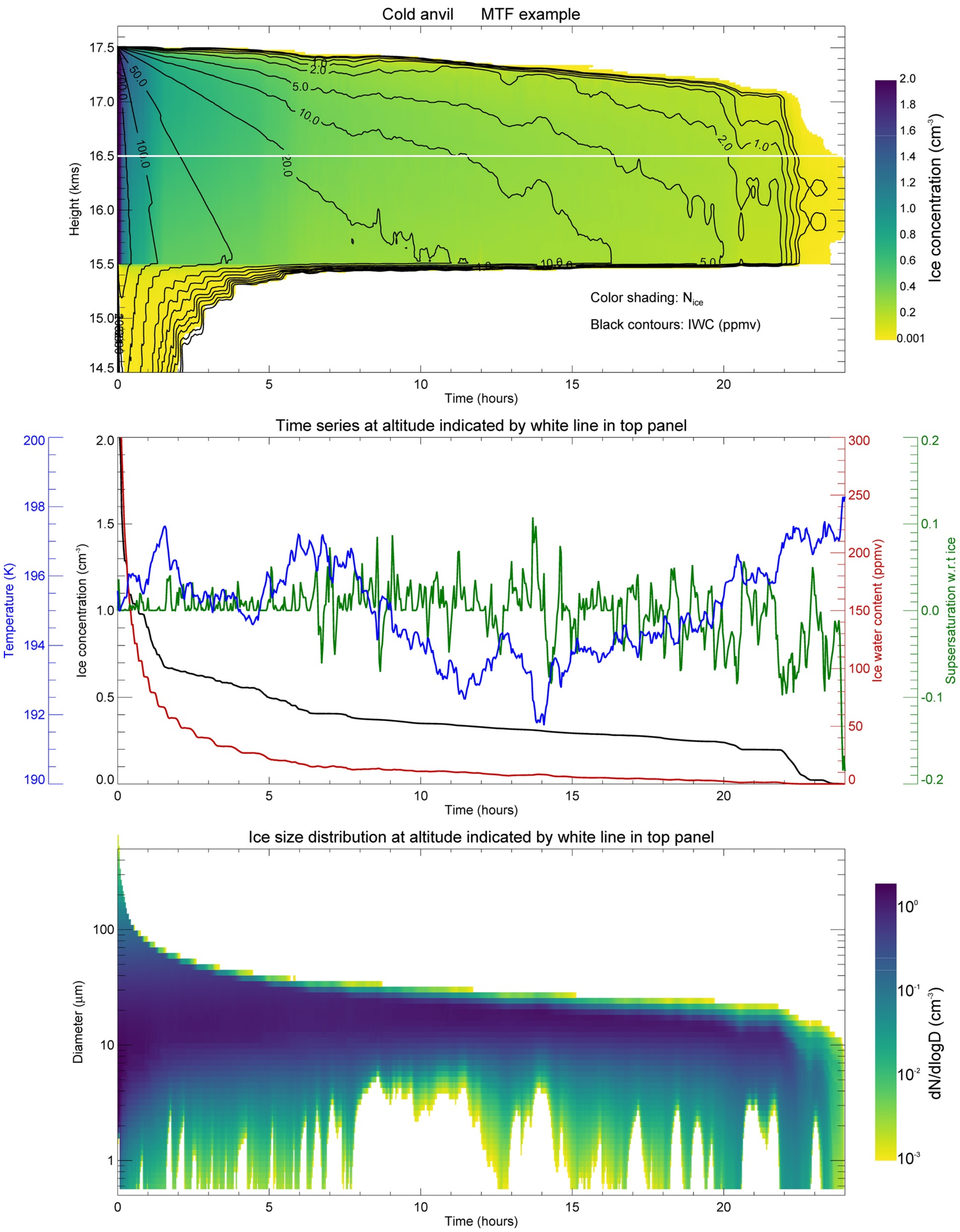

Figure 13. Results from a high/cold anvil simulation with a single realization of a mesoscale temperature fluctuation time series. Top panel: the cloud ice concentration (shading) and ice water content (IWC) (black contours) are shown versus time and height. Middle panel: time series of temperature (blue), ice supersaturation (green), ice concentration (black), and ice water content (red). Fields are shown at the altitude indicated by the horizontal white line in the top panel (16.5 km). Bottom panel: ice concentration versus time and crystal diameter at 16.5 km.

10.1029/2023JD039887

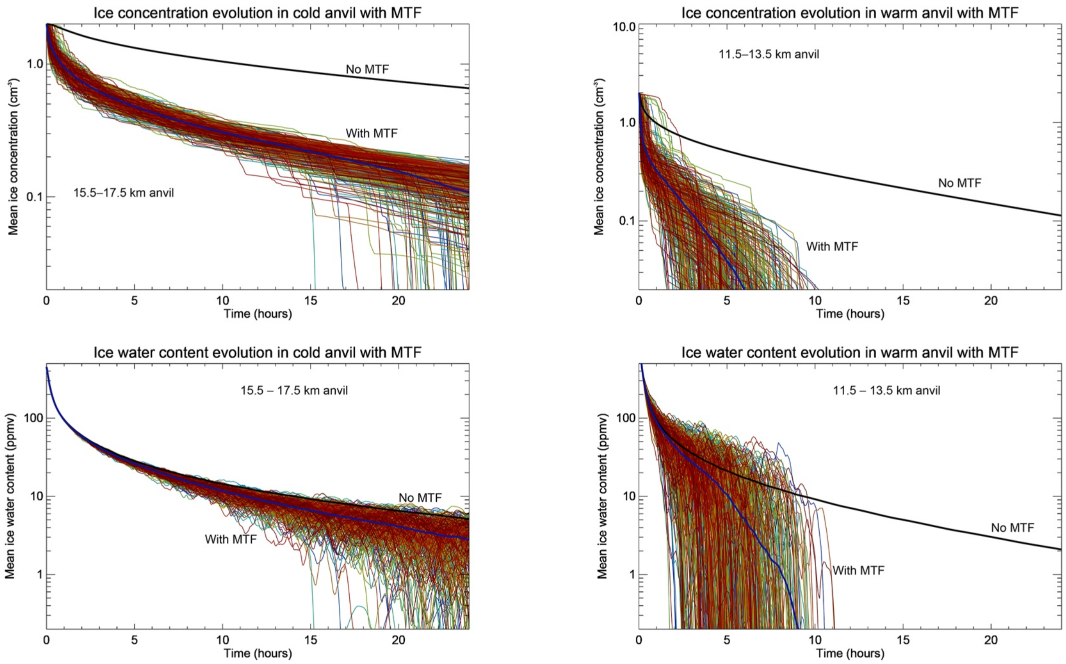

Figure 14. The vertically-averaged ice concentration (top panels) and ice water content (bottom panels) are plotted versus time for the high/cold anvil case (left panels) and for the low/warm anvil case (right panels). The thick solid black curves correspond to a simulation with no mesoscale temperature fluctuation (MTF), and the colored curves are individual simulations with different MTF time series. The thick blue curves are the ensemble means of the simulations with MTF.

In the case of the low anvil at 4–6 hr (right panel in Figure 16), the impact of MTF is even more pronounced even though we are showing results at an earlier simulation time. With MTF and the Kelvin effect, the mean ice concentration is reduced to about 100 L^{-1} by 4–6 hr. Even without the Kelvin effect, ice concentrations are reduced by MTF compared to the simulation with no waves.

8. Summary and Discussion

In this paper, we have addressed the impacts of temperature fluctuations driven by gravity waves on the evolution of ice crystal microphysical properties in evolving tropical anvil cirrus. We presented measurements from high-altitude aircraft campaigns showing the loss of small and large ice crystals in aging anvils. We used a one-dimensional model to investigate the interactions between gravity waves, deposition growth, sublimation, and sedimentation in evolving anvil cirrus. The effects of both coherent, monochromatic gravity waves and stochastic temperature fluctuations were evaluated. We simulated two anvil cirrus types: high/cold anvils in the uppermost tropical troposphere (15.5–17.5 km) and low/warm anvils at the primary tropical deep convection detrainment altitude (11.5–13.5 km). Key results are summarized as follows:

- In situ measurements with high-altitude aircraft show that active convection and fresh outflow contain both abundant small ice crystals (diameters less than 20 μm) as well as large ice crystals (diameters approaching 1 mm). In aged anvils, both the small and large crystals are absent.
- Modeling results indicate that either monochromatic waves or stochastic temperature fluctuations accelerate the loss of small ice crystals in anvil cirrus.
- The wave-induced reduction of ice concentration is a result of interaction between multiple physical processes, including deposition growth, sublimation, the Kelvin effect, and sedimentation.
- The Kelvin effect (higher vapor pressure over curved surfaces) drives mass transfer from small to large crystals. Without the Kelvin effect, the impact of waves on ice concentrations is much less significant, particularly for the high/cold anvil case.
- Anvil IWC in the early stages of anvil cirrus evolution is generally controlled by sedimentation loss of large crystals, but wave effects contribute to accelerated mass loss at later times, particularly for the low/warm anvil case.

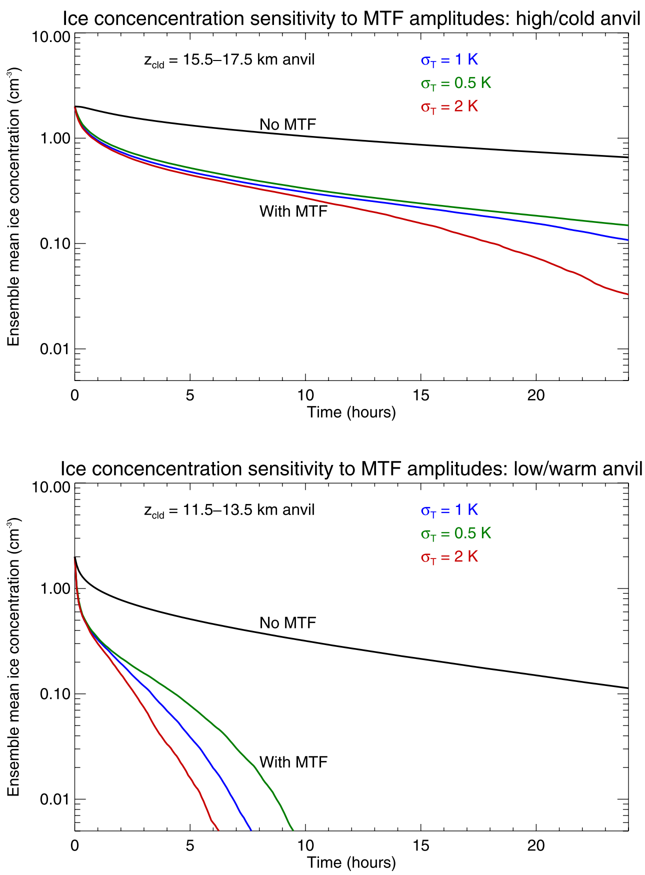

Figure 15. Time series of ensemble-mean, vertically-averaged ice concentration are plotted for simulations with the baseline mesoscale temperature fluctuation (MTF) temperature variance (1 K, blue curves), doubled variance (red curves), and halved variance (green curves). For comparison, the black curves show results from simulations without waves. The top panel shows results from the high/cold anvil, and the bottom panel shows results for the low/warm anvil.

- The wave-induced loss of small crystals, along with the sedimentation loss of large crystals, leaves a relatively narrow ice crystal size distribution with diameters ranging from about 10 to 20 μm.
- The wave-induced reduction of ice concentrations is much faster for lower (warmer) anvils because deposition growth and sublimation rates increase with increasing temperature. Waves generally drive complete sublimation of the low/warm anvils within several hours. Given this temperature dependence, wave effects will be more important for typical, relatively warm anvils detraining at ≃11–13 km than for rare, cold, TTL-penetrating anvils with tops near the tropical tropopause.
- The combination of waves and the Kelvin effect drives growth of crystals with initial diameters of ≃3–10 μm to sizes of 20–30 μm. This process is consistent with the appearance of bullet rosettes in aging anvil cirrus.

As noted above, previous modeling studies investigated the influence of waves on ice nucleation and showed that high-frequency gravity waves can enhance ice concentrations in cirrus (Corcos et al., 2023; Jensen et al., 2010; Spichtinger & Krämer, 2013). Here, we show that the influence of waves after ice nucleation has ceased is to decrease ice concentrations. We also note that other physical processes, such as entrainment dilution and small crystal sublimation driven by entrainment of dry air will reduce ice concentrations in evolving anvil cirrus. Also, we focused on wave-driven temperature fluctuations here, but processes such as radiatively driven small-scale convection and turbulence will also generate temperature variability within anvil cirrus. The overall lifetime of anvil cirrus is no doubt strongly affected by cloud-scale mesoscale circulations and synoptic-scale meteorological support. As a follow-on study, cloud resolving model simulations of convection and anvil cirrus could be used to realistically represent waves generated by the deep convection as well as dynamics driven by latent and radiative heating in the evolving anvil.

The transition to predominantly bullet rosette habits in anvil cirrus has been shown to require deposition growth of ice crystals under upper tropospheric conditions, and the results here suggest waves can enhance growth of mid-sized ice crystals. Laboratory studies have also shown that the transition

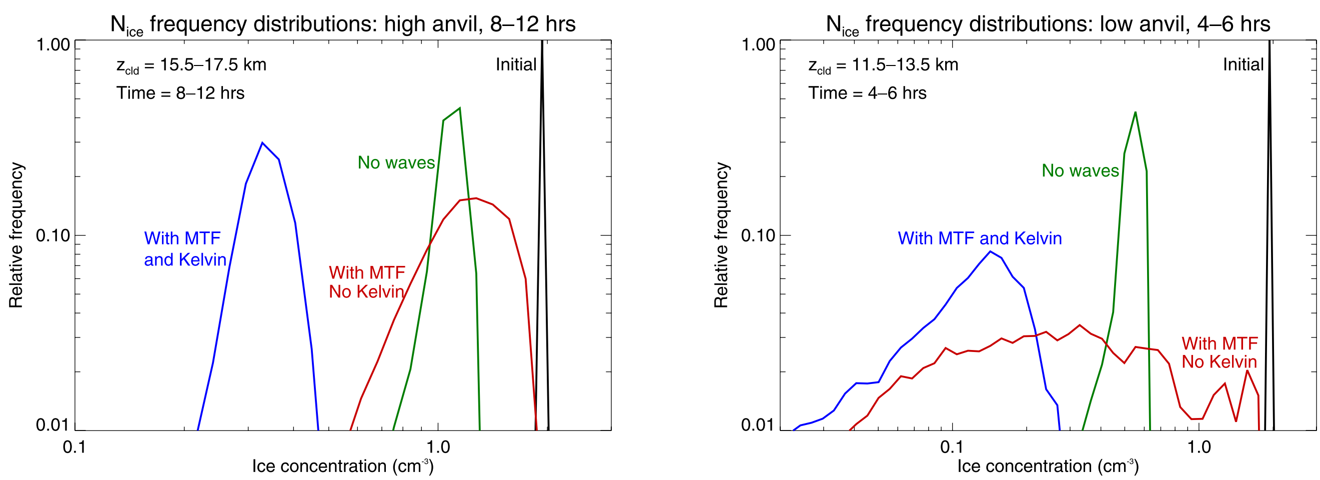

Figure 16. Frequency distributions of ice concentration. Left panel: results from high anvil simulations averaged over simulation times 8–12 hr. Right panel: results from low anvil simulations at 4–6 hr. The different colored curves show results from simulations with no mesoscale temperature fluctuation (MTF) (green), with MTF and including the Kelvin effect (blue), and with MTF but no Kelvin effect (red). The black curve shows the initial ice concentration (2 cm^{-3}). Note the different abscissa ranges for the left and right panels.

from pristine habits (such as plates and columns) to complex habits (such as bullet rosettes) only happens when the supersaturation exceeds a threshold value (Bailey & Hallett, 2004). At upper tropospheric temperatures, this threshold supersaturation is on the order of 20%. In situ measurements have shown that substantial supersaturations do occur within tropical cirrus clouds (Jensen, Thornberry, et al., 2017; Rollins et al., 2016), and these supersaturations are also primarily driven by the wave-driven temperature fluctuations that are prevalent in the upper troposphere.

We focused here on anvil cirrus produced by tropical deep convection. However, high-frequency gravity waves, along with the Kelvin effect, may be important for other types of cirrus as well. Optically thin cirrus formed in situ in the TTL generally have relatively small ice crystals (Woods et al., 2018), and the Kelvin effect is likely important for the evolution of ice crystal size distributions, particularly in the early stages of the cloud lifecycle after homogeneous freezing events when very small ice crystals predominate (Jensen et al., 2022). Since midlatitude cirrus form at higher temperatures than cirrus in the tropical upper troposphere, the wave-driven growth and sublimation processes will be faster and have a more pronounced impact on the cloud evolution. These issues will be addressed in a follow-on study.

The high-frequency waves discussed in this study are essentially absent in typical global climate models with horizontal grid spacings of 10 s of km and vertical resolutions on the order of 500 m. Recently, a number of global models have been run with horizontal grid resolution better than 5 km. However, Atlas and Bretherton (2023) recently showed that most of these global storm-resolving models also substantially under-predict the small-scale gravity wave activity. This deficiency represents another limitation in the ability of global models to realistically simulate cirrus clouds.

Data Availability Statement

The NASA airborne measurements of temperature, pressure, and water vapor, and cloud properties from the ATTREX and POSIDON campaigns are available from ATTREX (2014) and POSIDON (2016), respectively. The StratoClim measurements used here available from StratoClim (2016).

Acknowledgments

This work was supported by the NOAA Earth Radiation Budget Initiative. Additional support was provided by NASA Grants 80NSSC20K1235, 80NSSC23K1294, and NNA10DF71C. S. Woods was also supported by the National Center for Atmospheric Research and the National Science Foundation under Cooperative Agreement No. 1852977.

References

Atlas, R., & Bretherton, C. S. (2023). Aircraft observations of gravity wave activity and turbulence in the tropical tropopause layer: Prevalence, influence on cirrus clouds, and comparison with global storm-resolving models. *Atmospheric Chemistry and Physics*, *23*(7), 4009–4030. https://doi.org/10.5194/acp-23-4009-2023

ATTREX. (2014). The NASA Airborne Tropical Tropopause Experiment [Dataset]. NASA Earth Sciences Project Office. Retrieved from https://espoarchive.nasa.gov/archive/browse/attrex

Bailey, M., & Hallett, J. (2004). Growth rates and habits of ice crystals between –20° and –70°C. *Journal of the Atmospheric Sciences*, *61*(5), 514–544. https://doi.org/10.1175/1520-0469(2004)061<0514:grahoi>2.0.co;2

Bardeen, C. G., Toon, O. B., Jensen, E. J., Marsh, D., & Harvey, V. L. (2008). Numerical simulations of the three-dimensional distribution of meteoric dust in the mesosphere and upper stratosphere. *Journal of Geophysical Research*, *113*(D17202), 1–15. https://doi.org/10.1029/2007JD009515

Boehm, M. T., & Verlinde, J. (2000). Stratospheric influence on upper tropospheric tropical cirrus. *Geophysical Research Letters*, *27*(19), 3209–3212. https://doi.org/10.1029/2000gl011678

Boehm, M. T., Verlinde, J., & Ackerman, T. P. (1999). On the maintenance of high tropical cirrus. *Journal of Geophysical Research*, *104*(D20), 24423–24433. https://doi.org/10.1029/1999jd900798

Corcos, M., Hertzog, A., Ploughonven, R., & Podglajen, A. (2021). Observation of gravity waves at the tropical tropopause using superpressure balloons. *Journal of Geophysical Research: Atmospheres*, *126*(15), e2021JD035165. https://doi.org/10.1029/2021JD035165

Corcos, M., Hertzog, A., Ploughonven, R., & Podglajen, A. (2023). A simple model to assess the impact of gravity waves on ice-crystal populations in the tropical tropopause layer. *Atmospheric Chemistry and Physics*, *23*(12), 6923–6939. https://doi.org/10.5194/acp-23-6923-2023

Costa, A., Meyer, J., Afchine, A., Luebke, A., Günther, G., Dorsey, J. R., et al. (2017). Classification of Arctic, midlatitude and tropical clouds in the mixed-phase temperature regime. *Atmospheric Chemistry and Physics*, *17*(19), 12219–12238. https://doi.org/10.5194/acp-17-12219-2017

Dinh, T. P., Podglajen, A., Hertzog, A., Legras, B., & Plougonven, R. (2016). Effect of gravity wave temperature fluctuations on homogeneous ice nucleation in the tropical tropopause layer. *Atmospheric Chemistry and Physics*, *16*(1), 35–46. https://doi.org/10.5194/acp-16-35-2016

Gallagher, M. W., Connolly, P. J., Crawford, I., Heymsfield, A., Bower, K. N., Choularton, T. W., et al. (2012). Observations and modelling of microphysical variability, aggregation and sedimentation in tropical anvil cirrus outflow regions. *Atmospheric Chemistry and Physics*, *12*(14), 6609–6628. https://doi.org/10.5194/acp-12-6609-2012

Gasparini, B., Blossey, P. N., Hargmann, D. L., Lin, G., & Fan, J. (2019). What drives the life cycle of tropical anvil clouds? *Journal of Advances in Modeling Earth Systems*, *11*(8), 2586–2605. https://doi.org/10.1029/2019MS001736

Immler, F., Krüger, K., Fujiwara, M., Verver, G., Rex, M., & Schrems, O. (2008). Correlation between equatorial kelvin waves and the occurrence of extremely thin ice clouds at the tropical tropopause. *Atmospheric Chemistry and Physics*, *8*(14), 4019–4026. https://doi.org/10.5194/acp-8-4019-2008

Jensen, E. J., & Ackerman, A. S. (2006). Homogeneous aerosol freezing in the tops of high-altitude tropical cumulonimbus clouds. *Geophysical Research Letters*, *33*(8), L08802. https://doi.org/10.1029/2005GL024928

Jensen, E. J., Diskin, G., DiGangi, J., Woods, S., Lawson, R. P., & Bui, T. V. (2022). Homogeneous freezing events sampled in the Tropical Tropopause Layer. *Journal of Geophysical Research: Atmospheres*, *127*(17), e2022JD036535. https://doi.org/10.1029/2022JD036535

Jensen, E. J., Lawson, P., Baker, B., Pilson, B., Mo, Q., Heymsfield, A., et al. (2009). On the importance of small ice crystals in tropical anvil cirrus. *Atmospheric Chemistry and Physics*, *9*(15), 5519–5537. https://doi.org/10.5194/acp-9-5519-2009

Jensen, E. J., Pfister, L., Bui, T.-P., Lawson, P., & Baumgardner, D. (2010). Ice nucleation and cloud microphysical properties in tropical tropopause cirrus. *Atmospheric Chemistry and Physics*, *10*(3), 1369–1384. https://doi.org/10.5194/acp-10-1369-2010

Jensen, E. J., Pfister, L., Jordan, D. E., Bui, T. V., Ueyama, R., Singh, H. B., et al. (2017). The NASA Airborne Tropical TRopopause EXperiment (ATTREX): High-altitude aircraft measurements in the tropical western Pacific. *Bulletin America Meteorology Social*, *1*. https://doi.org/10.1175/BAMS-D-14-00263.1

Jensen, E. J., Thornberry, T. D., Rollins, A. W., Ueyama, R., Pfister, L., Bui, T., et al. (2017). Physical processes controlling the spatial distributions of relative humidity in the tropical tropopause layer over the Pacific. *Journal of Geophysical Research: Atmospheres*, *122*(11), 6094–6107. https://doi.org/10.1002/2017JD026632

Jensen, E. J., Toon, O. B., Drdla, K., & Tabazadeh, A. (2002). Impact of polar stratospheric cloud particle composition, number density, and lifetime on denitrification. *Journal of Geophysical Research*, *107*(D20), 8284. https://doi.org/10.1029/2001JD000440

Jensen, E. J., Ueyama, R., Pfister, L., Bui, T. V., Alexander, M. J., Podglajen, A., et al. (2016). High-frequency gravity waves and homogeneous ice nucleation in tropical tropopause layer cirrus. *Geophysical Research Letters*, *43*(12), 6629–6635. https://doi.org/10.1002/2016GL069426

Jensen, E. J., van den Heever, S. C., & Grant, L. D. (2018). The lifecycles of ice crystals detrained from the tops of deep convection. *Journal of Geophysical Research: Atmospheres*, *123*(17), 9624–9634. https://doi.org/10.1029/2018jd028832

Kärcher, B., Jensen, E. J., Pokrifka, G. F., & Harrington, J. Y. (2023). Ice supersaturation variability in cirrus clouds: Role of vertical wind speeds and deposition coefficients. *Journal of Geophysical Research: Atmospheres*, *128*(22), e2023JD039324. https://doi.org/10.1029/2023jd039324

Kärcher, B., & Podglajen, A. (2019). A stochastic representation of temperature fluctuations induced by mesoscale gravity waves. *Journal of Geophysical Research: Atmospheres*, *124*(21), 11506–11529. https://doi.org/10.1029/2019JD030680

Karoly, D. J., Roff, G. L., & Reeder, M. J. (1996). Gravity wave activity associated with tropical convection detected in toga coare sounding data. *Geophysical Research Letters*, *23*(3), 261–264. https://doi.org/10.1029/96gl00023

Kim, J.-E., Alexander, M. J., Bui, T. P., Dean-Day, J. M., Lawson, R. P., Woods, S., et al. (2016). Ubiquitous influence of waves on tropical high cirrus cloud. *Geophysical Research Letters*, *43*(11), 5895–5901. https://doi.org/10.1002/2016GL069293

Krämer, M., Rolf, C., Luebke, A., Afchine, A., Spelten, N., Costa, A., et al. (2016). A microphysics guide to cirrus clouds - Part 1: Cirrus types. *Atmospheric Chemistry and Physics*, *16*(5), 3463–3483. https://doi.org/10.5194/acp-16-3463-2016

Krämer, M., Rolf, C., Spelten, N., Afchine, A., Fahey, D., Jensen, E., et al. (2020). A microphysics guide to cirrus - Part II: Climatologies of clouds and humidity from observations. *Atmospheric Chemistry and Physics*, *20*, 20. https://doi.org/10.5194/acp-20-12569-2020

Krämer, M., Schiller, C., Afchine, A., Gensch, I., Mangold, A., Spelten, N., et al. (2009). Ice supersaturations and cirrus cloud crystal numbers. *Atmospheric Chemistry and Physics*, *9*(11), 3505–3522. https://doi.org/10.5194/acp-9-3505-2009

Lamraoui, F., Krämer, M., Afchine, A., Sokol, A. B., Khaykin, S., Pandey, A., & Kuang, Z. (2023). Sensitivity of convectively driven tropical tropopause cirrus properties to ice habits in high-resolution simulations. *Atmospheric Chemistry and Physics*, *23*(4), 2393–2419. https://doi.org/10.5194/acp-23-2393-2023

Lane, T. P., Reeder, M. J., & Clark, T. L. (2001). Numerical modeling of gravity wave generation by deep tropical convection. *Journal of the Atmospheric Sciences*, *58*(10), 1249–1274. https://doi.org/10.1175/1520-0469(2001)058<1249:nmogwg>2.0.co;2

Lawson, R. P., Woods, S., Jensen, E., Erfani, E., Gurganus, C., Gallagher, M., et al. (2019). A review of ice particle shapes in cirrus formed in situ and in anvils. *Journal of Geophysical Research: Atmospheres*, *124*(17–18), 10049–10090. https://doi.org/10.1029/2018JD030122

Luo, Z., & Rossow, W. B. (2004). Characterizing tropical cirrus life cycle, evolution, and interaction with upper-tropospheric water vapor using Lagrangian trajectory analysis of satellite observations. *Journal of the Atmospheric Sciences*, *17*(23), 4541–4563. https://doi.org/10.1175/3222.1

Mace, G. G., Deng, M., Soden, B., & Zipser, E. (2006). Association of tropical cirrus in the 10-15-km layer with deep convective sources: An observational study combining millimeter radar data and satellite-derived trajectories. *Journal of the Atmospheric Sciences*, *63*(2), 480–503. https://doi.org/10.1175/jas3627.1

McFarquhar, G. M., Um, J., Freer, M., Baumgardner, D., Kok, G. L., & Mace, G. (2007). The importance of small ice crystals to cirrus properties: Observations from the Tropical Warm Pool International Cloud Experiment (TWP-ICE). *Geophysical Research Letters*, *57*(L13803), 1–6. https://doi.org/10.1029/2007GL029865

Nath, D., Ratnam, M. V., Rao, V. V. M. J., Murthy, B. V. K., & Rao, S. V. B. (2009). Gravity wave characteristics observed over a tropical station using high-resolution GPS radiosonde soundings. *Journal of Geophysical Research*, *114*(D6), 1–12. https://doi.org/10.1029/2008JD011056

Podglajen, A., Bui, T. P., Dean-Day, J. M., Pfister, L., Jensen, E. J., Alexander, M. J., et al. (2017). Small-scale wind fluctuations in the tropical tropopause layer from aircraft measurements: Occurrence, nature and impact on vertical mixing. *Journal of the Atmospheric Sciences*, *74*(11), 3847–3869. https://doi.org/10.1175/JAS-D-17-0010.1

Podglajen, A., Hertzog, A., Plougonven, R., & Legras, B. (2016). Lagrangian temperature and vertical velocity fluctuations due to gravity waves in the lower stratosphere. *Geophysical Research Letters*, *43*(7), 3543–3553. https://doi.org/10.1002/2016GL068148

Podglajen, A., Plougonven, R., Hertzog, A., & Jensen, E. (2018). Impact of gravity waves on the motion and distribution of atmospheric ice particles. *Atmospheric Chemistry and Physics*, *18*(14), 10799–10823. https://doi.org/10.5194/acp-18-10799-2018

POSIDON. (2016). The Pacific Oxidants, Sulfur, Ice, Dehydration, and cONvection Experiment [Dataset]. NASA Earth Sciences Project Office. Retrieved from https://espoarchive.nasa.gov/archive/browse/posidon

Rollins, A. W., Thornberry, T. D., Gao, R. S., Woods, S., Lawson, R. P., Bui, T. P., et al. (2016). Observational constraints on the efficiency of dehydration mechanisms in the tropical tropopause layer. *Geophysical Research Letters*, *43*(6), 2912–2918. https://doi.org/10.1002/2016GL067972

Scott, S. G., Bui, T. P., Chan, K. R., & Bowen, S. W. (1990). The Meteorological Measurement System on the NASA ER-2 aircraft. *Journal of Atmospheric and Oceanic Technology*, *7*(4), 525–540. https://doi.org/10.1175/1520-0426(1990)007<0525:tmmsot>2.0.co;2

Seeley, J. T., Jeevanjee, N., Langhans, W., & Romps, D. M. (2019). Formation of tropical anvil clouds by slow evaporation. *Geophysical Research Letters*, *46*(1), 492–501. https://doi.org/10.1029/2018GL080747

Spichtinger, P., & Krämer, M. (2013). Tropical tropopause ice clouds: A dynamic approach to the mystery of low crystal numbers. *Atmospheric Chemistry and Physics*, *13*(19), 9801–9818. https://doi.org/10.5194/acp-13-9801-2013

StratoClim. (2016). Stratospheric and upper tropospheric processes for better climate predictions [Dataset]. Deutches Zentrum für Lüft und Raumfahrt HALO database. Retrieved from https://halo-db.pa.op.dlr.de/mission/101

Toon, O. B., Turco, R. P., Westphal, D., Malone, R., & Liu, M. S. (1988). A multidimensional model for aerosols: Description of computational analogs. *Journal of the Atmospheric Sciences*, *45*(15), 2123–2143. https://doi.org/10.1175/1520-0469(1988)045<2123:ammfad>2.0.co;2

Vincent, R., & Alexander, M. J. (2000). Gravity waves in the tropical lower stratosphere: An observational study of seasonal and interannual variability. *Journal of Geophysical Research*, *105*(D14), 17971–17982. https://doi.org/10.1029/2000jd900196

Woods, S., Lawson, R. P., Jensen, E. J., Bui, P., Thornberry, T., Rollins, A., et al. (2018). Microphysical properties of tropical tropopause layer (TTL) cirrus. *Journal of Geophysical Research: Atmospheres*, *123*(11), 6053–6069. https://doi.org/10.1029/2017JD028068

Yuan, J., & Houze, R. (2010). Global variability of mesoscale convective system anvil structure from A-train satellite data. *Journal of Climate*, *23*(21), 5864–5888. https://doi.org/10.1175/2010JCLI3671.1